

# Mass and energy balance calculations for an artificial ice reservoir (Icestupa)

Suryanarayanan Balasubramanian<sup>1,\*</sup>, Martin Hoelzle<sup>1</sup>, Michael Lehning<sup>2</sup>,  
Sonam Wangchuk<sup>3</sup>, Johannes Oerlemans<sup>4</sup> and Felix Keller<sup>5</sup>

<sup>1</sup> University of Fribourg, Fribourg, Switzerland

<sup>2</sup> WSL Institute for Snow and Avalanche Research, Davos, Switzerland

<sup>3</sup> Himalayan Institute of Alternatives Ladakh, Leh, India

<sup>4</sup> Institute for Marine and Atmospheric Research, Utrecht University, Utrecht, The Netherlands

<sup>5</sup> Academia Engiadina, Samedan, Switzerland

Correspondence\*:

Suryanarayanan Balasubramanian

suryanarayanan.balasubramanian@unifr.ch

## 2 ABSTRACT

Artificial Ice Reservoirs (AIR) have been successful in storing water during winter and releasing the water during spring and summer. This has made them a reliable fresh water resource for irrigation in dry environments. Several AIRs have been built but studies of their water storage capacity and efficiency are scarce. This study attempts to model a cone-shaped AIR popularly called Icestupa. Important processes involved in the development and temporal evolution of an Icestupa are calculated by a physically-based model using equations governing the heat transfer, vapour diffusion and transport of water that undergoes phase changes. These processes were quantified using meteorological data in conjunction with fountain spray information (mass input of an Icestupa) to estimate the quantity of frozen, melted, evaporated and drained water at a location called 'Eispalast' in Fribourg, Switzerland. At this measurement site, an Icestupa was built for model validation purposes. The model was further tested by performing sensitivity and uncertainty study showing that the most sensitive parameters are the ice emissivity and the temperature threshold used to determine precipitation phase. Model calculations estimate that the Schwarzsee Icestupa stored about 8% of the total water sprayed as ice. In addition, we found that reducing nozzle diameter of the fountain to 3 mm increases the storage efficiency up to 93% without compromising on the storage duration.

Keywords: ictestupa, mass balance, water storage, climate change adaptation, geoengineering

## 1 INTRODUCTION

Seasonal snow cover, glaciers and permafrost are expected to change their water storage capacity due to climate change with major consequences for downriver water supply (Immerzeel et al., 2019). The challenges brought about by these changes are especially important for dry mountain environments such as in Central Asia or the Andes, which directly rely on the seasonal meltwater for their farming and drinking needs (Hoelzle et al., 2019; Apel et al., 2018; Buytaert et al., 2017; Chen et al., 2016; Unger-Shayesteh



**Figure 1.** Icestupa in Ladakh, India on March 2017 was 24 m tall and contained around 3.7 million litres of water. Picture Credits: Lobzang Dadul

25 et al., 2013). Some villages in Ladakh, India have already been forced to relocate due to glacial retreat and  
26 the corresponding loss of their main fresh water resources (Grossman, 2015).

27 AIRs have been considered to be a feasible way to adapt to these changes (Hock et al., 2019; Nüsser  
28 et al., 2019b). An artificial ice reservoir is a human-made ice structure typically constructed during the  
29 cold winter months and designed to slowly release freshwater during the warm and dry spring and summer  
30 months. The main purpose of AIR is irrigation. Therefore, AIRs are designed to store water in the form of  
31 ice as long into the summer as possible. The energy required to construct an AIR is usually derived from  
32 the gravitational head of the source water body. Some are constructed horizontally by freezing water using  
33 a series of checkdams and others are built vertically by spraying water through fountain systems (Nüsser  
34 et al., 2019a). The latter are colloquially referred to as Icestupas and are the subject of this study.

35 Since their invention in 2013 (Wangchuk, 2014), Icestupas have gained widespread publicity in the region  
36 of Ladakh, Northern India since they require very little infrastructure, skills and energy to be constructed  
37 in comparison to other water storage technologies. Compared to other AIR geometries, Icestupas (Fig.  
38 1) can be built at lower altitudes and last much longer into the summer than other types of ice structures  
39 (Wangchuk, 2014).

40 A typical Icestupa just requires a pipeline attached to a vertically mounted metal pipe with a fountain  
41 nozzle for construction. Water source is usually a high altitude lake or glacial stream. Due to the altitude  
42 difference between the pipeline input and fountain output, water ejects from the fountain nozzle as droplets  
43 that eventually lose their latent heat to the atmosphere and accumulate as ice around the metal pipe.  
44 The fountain nozzle is raised through addition of further pipes as and when significant ice accumulates.  
45 Typically, a dome of branches is constructed around the metal pipe so that such pipe extensions can be  
46 done from within this dome. During the winter, the fountain is manually activated between sunset and  
47 sunrise. Threads, tree branches and fishing nets are used to guide and accelerate the ice formation.

48 If AIR are to become a viable water resource management tool, it is crucial to be able to propose suitable  
49 construction sites, and to identify and minimize water losses. However, to date, no reliable estimates exist  
50 about the amount of sprayed water that is necessary to create them and the meltwater they provide (Nüsser  
51 et al., 2019a). Rough estimates of Icestupa meltwater in Ladakh suggest that the water loss during the

52 construction process is considerable (see Appendix 8.1). A complete set of measurements of the water  
 53 storage and energy balance are required to understand the cause of the water losses better and increase the  
 54 construction efficiency.

55 In this paper, we aim to develop a physically-based model of a vertical AIR (or Icestupa) that can quantify  
 56 their storage efficiency using existing weather and water usage information. Mass and energy balance  
 57 equations were used to estimate the quantity of water frozen, melted, evaporated and drained. Sensitivity  
 58 and uncertainty analysis were performed to identify the most critical parameters and the variance caused  
 59 by them. For validation, we created an Icestupa at an accessible site (called Eispalast) near Schwarzsee in  
 60 the Canton of Fribourg, Switzerland, allowing easy maintenance and control of the measurements. Due  
 61 to the low altitude of the site with relatively high winter temperatures, only a small Icestupa could be  
 62 established during winter 2018/19 for providing us with model validation data. Our model and validation  
 63 experiments provide first steps towards evaluating the effectiveness of a vertical AIR for irrigation and  
 64 finally we outline some preliminary guidelines for consideration when a construction of an Icestupa for  
 65 water storage is envisaged.

## 2 STUDY SITE

66 The Eispalast site in the Schwarzsee region lies at 967 m a.s.l. In the winter (Oct-Apr), mean daily  
 67 maximum and minimum air temperatures vary between 14 to -4 °C. Clear skies are rare, averaging around  
 68 7 days, and precipitation amounts average 155 mm per month during winter (Meteoblue, 2020). The site  
 69 was situated adjacent to a stream resulting in high humidity values across the study period. Within the  
 70 Eispalast site, 1.8 m in radius enclosure was constructed for the experiment. An automatic weather station  
 71 (AWS) was set in place adjacent to the wooden boundary as shown in Fig. 2. The fountain used for spraying  
 72 water had a nozzle diameter of 5 mm and a height of 1.35 m, and was placed in the centre of the wooden  
 73 enclosure. The water was transferred from a spring water source at 1267 m a.s.l. by pipeline and flowed  
 74 via a flowmeter and an air escape valve to the nozzle, where it was sprinkled with a spray radius of around  
 75 1.7 m. The air escape valve was installed to avoid errors in the flow measurements due to air bubbles. In  
 76 addition, a webcam guaranteed a continuous survey of the site during the construction of the Icestupa.

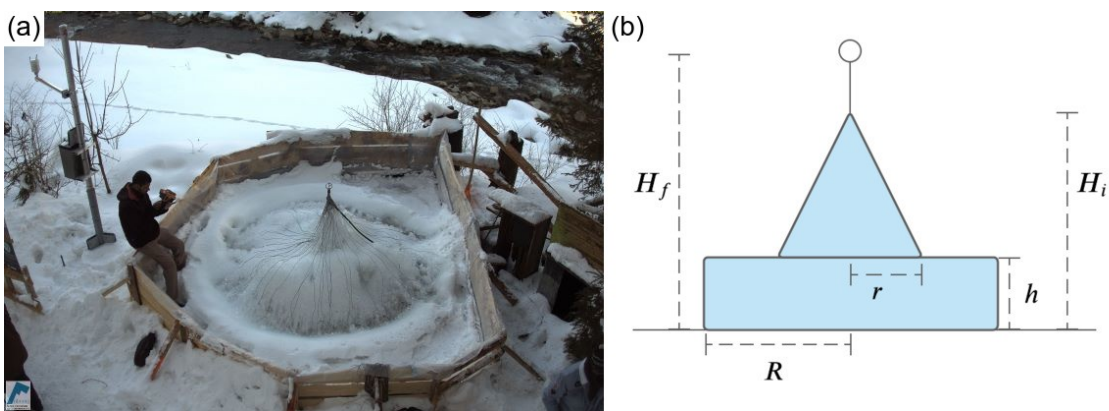


**Figure 2.** (a) The ice structure during the first validation measurement as seen on the webcam image of 14<sup>th</sup> Feb. (b) The corresponding cross section of the Schwarzsee ice structure with the field estimates of  $r, R, h, H_i, H_f$  used to determine the Icestupa volume is shown on the right.

77 **2.1 Construction**

78 From 30<sup>th</sup> January to 18<sup>th</sup> March 2019 the Icestupa was constructed through the fountain spray, which  
 79 was manually switched on if measured air temperature was below -5 °C after sunset and was switched  
 80 off as soon as the ice was exposed to daylight or temperatures were above 0 °C. The water spray of the  
 81 fountain was initially adjusted so that most of the water droplets land within the wooden boundary zone.  
 82 The ice formation was guided by adding a metal framework at the ice structure base after the first night of  
 83 operation. Several cotton threads were tied between the ice structure base and fountain pole for accelerating  
 84 and further guiding the ice formation process.

85 **2.2 Measurements and Data**

86 The Schwarzsee AWS was located at 967 m a.s.l. It was in operation from 30<sup>th</sup> January to 18<sup>th</sup> March  
 87 2019. Measurements comprise air temperature, relative humidity, water flow, wind speed and direction.  
 88 All these measurements were stored as 5 minute means. Precipitation data was derived from the Plaffeien  
 89 AWS (IDAWEB, 2019) located 8.8 km away from the measurement site at an altitude of 1042 m a.s.l.

90 ERA5 reanalysis dataset (Copernicus Climate Change Service (C3S), 2017) was used to obtain the rest of  
 91 the meteorological parameters. It has a horizontal resolution of approximately 30 km (Hersbach et al., 2020).  
 92 Direct and diffuse shortwave radiation were derived from ERA5 surface solar radiation downwards and  
 93 total sky direct solar radiation parameter. Total cloud cover parameter of ERA5 represented the cloudiness  
 94 index. The hourly ERA5 data and the 10 minute Plaffeien AWS data were linearly interpolated to the 5  
 95 minute data frequency of the Schwarzsee AWS.

96 Due to a power failure, all data from the Schwarzsee AWS was lost between 27<sup>th</sup> February 15:20 2019 to  
 97 2<sup>nd</sup> March 15:00 2019. Consequently, the amount of missing data in the dataset was around 7%. During  
 98 heavy snowfall events, the ultrasonic wind sensor was blocked and recorded zero values. To fill such  
 99 errors and data gaps, we used the ERA5 reanalysis dataset as it was better correlated with the associated  
 100 parameters in Schwarzsee compared to Plaffeien dataset. Namely, the 2m temperature parameter correlated  
 101 ( $r^2 =$ ) with air temperature, surface pressure parameter correlated ( $r^2 =$ ) with air pressure and 10m wind  
 102 speed parameter (derived from horizontal and vertical components) correlated ( $r^2 =$ ) with wind speed.  
 103 Near-surface humidity is not archived directly in ERA datasets, but from near-surface (2m from the surface)  
 104 temperature ( $T_{ERA5}$ ) and dew point temperature ( $Tw_{ERA5}$ ) one can calculate relative humidity( $RH$ ) at  
 105 2m as follows:

$$RH = 100 \cdot \frac{e_{sat}(Tw_{ERA5})}{e_{sat}(T_{ERA5})} \quad (1)$$

106 where the saturation vapour pressure function  $e_{sat}$  is expressed with the Teten's formula (Tetens, 1930):

$$e_{sat}(T) = a_1 \cdot e^{(a_3 \cdot \frac{T}{(T+273.16-a_4)})} \quad (2)$$

107 with T in °C and the parameters set for saturation over water ( $a_1 = 611.21$  Pa,  $a_3 = 17.502$  and  $a_4 = 32.19$   
 108 K) according to Buck (1981). Zero wind speed values were recorded whenever snow accumulated on the  
 109 ultrasonic wind sensor. So all null values were replaced using the ERA5 dataset.

110 The ERA5 grid point chosen (Latitude 46° 38' 24" N, Longitude 7° 14' 24" E) for the Schwarzsee site  
 111 was around 9 km away from the actual site. So all the ERA5 variables were fitted with the Schwarzsee  
 112 dataset via linear regressions. Through this modified ERA5 dataset, we were also able to further extend the  
 113 Schwarzsee dataset and allow the model to run beyond 18<sup>th</sup> March 2019. Precipitation was filled as null  
 114 values beyond 18<sup>th</sup> March 2019.

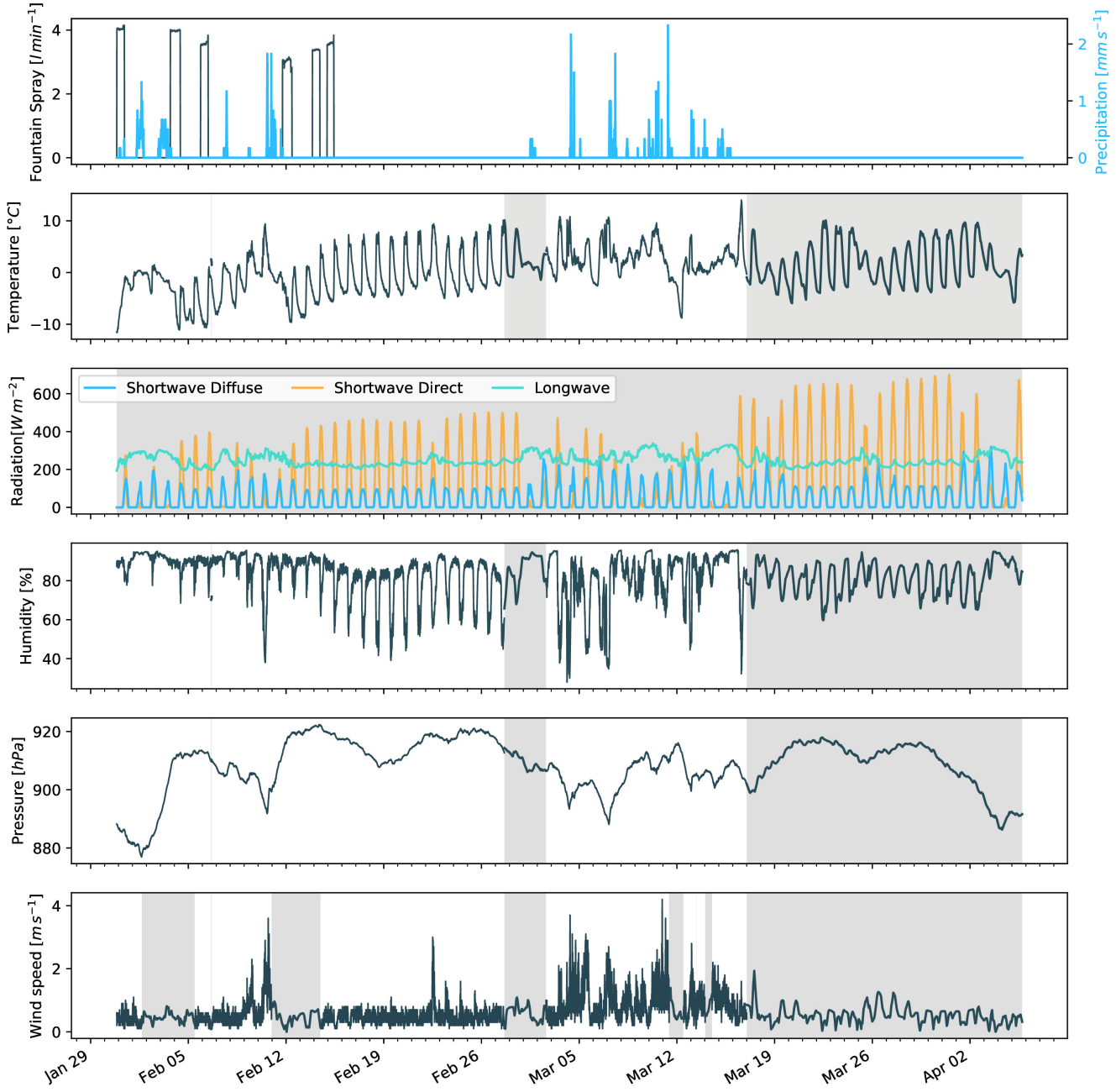


**Figure 3.** Measurements at the AWS of Schwarzsee (black) were used as main model input data in 5 minute frequency. Plaffeien AWS (blue) provided the precipitation data. Cloudiness and incoming shortwave radiation were obtained from the ERA5 reanalysis dataset (orange).

### 115 2.2.1 Field Measurements for validation

116 The volume was determined by decomposing the ice structure into a cylinder (length  $2R$  and height  $h$ )  
 117 and a cone (radius  $2r$  and height  $(H_i - h)$ ) through the following equation:

$$V = \pi * 2 * R * h + 1/3 * \pi * r^2 * H_i \quad (3)$$

118 Manual measurements were performed at the end of the freezing period on 14<sup>th</sup> February 16:00 2019  
 119 (only one more fountain run was possible after this date) to estimate  $r, R, h, H_i, H_f$  (see Fig. 2 for the  
 120 different geometry components):

$$0.55 \leq r \leq 1m ; 1.1 \leq R \leq 1.2m ; 0.1 \leq h \leq 0.2m ; 0.6 \leq H_i \leq 0.8m ; 1.3 \leq H_f \leq 1.4m$$

121 The ranges of the variables show its variance across different compass orientations. Correspondingly, the  
 122 volume range estimated for the first validation point was  $0.857 \pm 0.186 m^3$  on 14<sup>th</sup> February 16:00 2019.

123 The second validation point corresponds to the end of the melting process on 10<sup>th</sup> March 18:00 2019.  
 124 Based on the webcam imagery and manual measurement, a thin layer of ice with an observed thickness  
 125 between 0.01 to 0.06 m could be quantified. This results in the volume range for the second validation to  
 126 be  $0.13 \pm 0.09 m^3$  on 11<sup>th</sup> March 2019

127 In reality, the Schwarzsee ice structure was more cylindrical until a height of 0.2 m and conical afterwards  
 128 until a height of 0.6 m with a radius of 1.18 m. However, we assume a conical shape of this ice structure in  
 129 order to apply the modelling strategy described below.

### 3 MODEL SETUP

130 The model (implemented in python) consists of three parts calculating a) the geometric evolution of the  
 131 Icestupa, b) the energy balance and c) the mass balance as shown schematically in Fig. 4. A bulk energy  
 132 and mass balance model is used to calculate the amounts of ice, liquid water, water vapour and drained  
 133 water of the Icestupa every 5 minutes. The equations used henceforth display model time step superscript  
 134 only if it is different from the current time step.

#### 3.1 Icestupa geometric evolution

136 Radius  $r_{ice}$  and height  $h_{ice}$  define the dimensions of the Icestupa assuming its geometry to be a cone as  
 137 shown in Fig. 5. The surface area  $A$  exposed to the atmosphere and volume  $V$  are:

$$A = \pi \cdot r_{ice} \cdot \sqrt{r_{ice}^2 + h_{ice}^2} \quad (4)$$

$$V = \pi/3 \cdot r_{ice}^2 \cdot h_{ice} \quad (5)$$

138 With the mass of the Icestupa  $M_{ice}$ , its current volume can also be expressed as:

$$V = M_{ice}/\rho_{ice} \quad (6)$$

139 where  $\rho_{ice}$  is the density of ice ( $917 kg m^{-3}$ ). The model of the Icestupa is initialised with a thickness  
 140 of  $\Delta x$  (defined in 3.2) and a circular area of radius  $r_F$ . The constant  $r_F$  represents the mean spray radius  
 141 of the fountain. This fountain spray radius is determined by modelling the projectile motion of the water  
 142 droplets. Using mass conservation the droplet speed  $v_F$  can be determined from the spray rate  $d_F$  and the  
 143 diameter  $dia_F$  of the nozzle as follows:

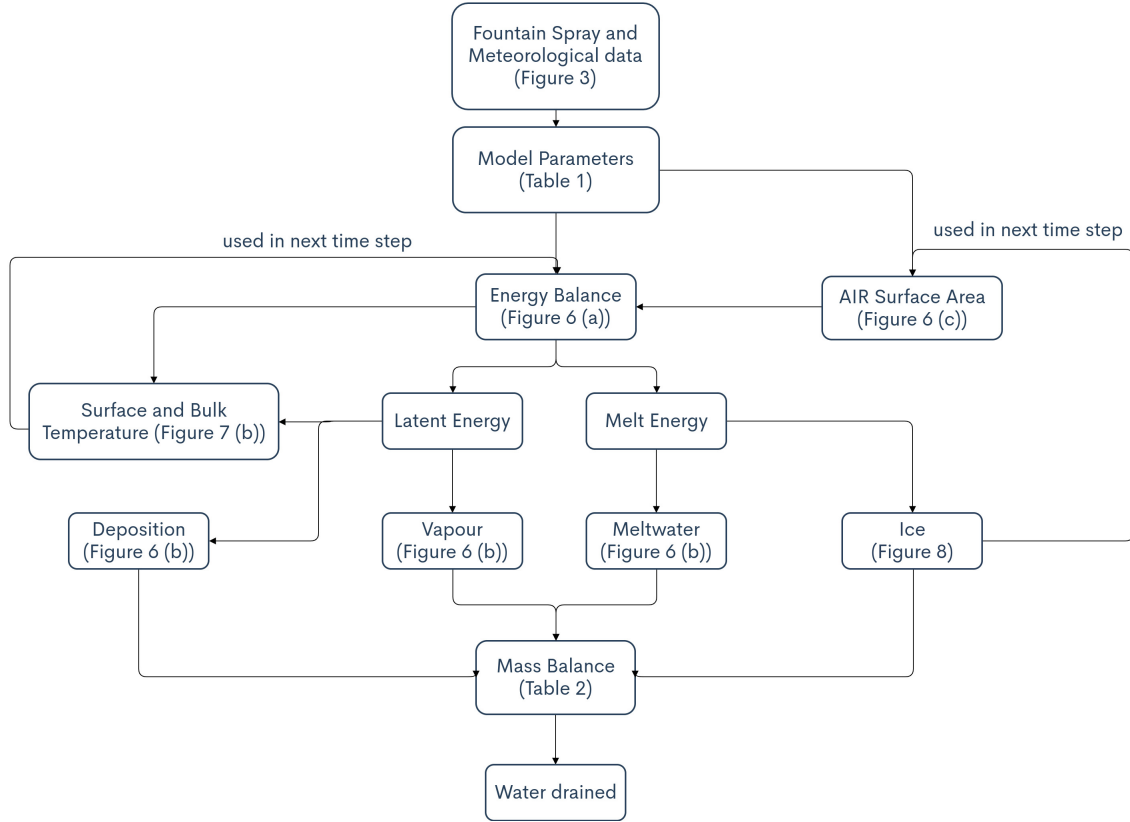


**Figure 4.** Model schematic showing the algorithm used in the model at every time step. Further details about these variables can be found in the associated tables and figures.

$$v_F = \frac{d_F}{\pi \cdot dia_F^2 / 4} \quad (7)$$

144 Afterwards, we assume that the water droplets move with an air friction free projectile motion from  
 145 the fountain nozzle with a height  $h_F$  to the ice/ground surface. The resulting spray radius  $r_F$  was then  
 146 determined from the projectile motion equation as follows:

$$r_F = \frac{v_F \cdot \cos\theta_F (v_F \cdot \sin\theta_F + \sqrt{(v_F \cdot \sin\theta_F)^2 + 2 \cdot g \cdot h_F})}{g} \quad (8)$$

147 where  $g = 9.8ms^{-2}$  is the acceleration due to gravity and  $\theta_F = 45^\circ$  is the angle of launch.

148 During subsequent time steps, the dimensions of the Icestupa evolve assuming a uniform ice formation  
 149 and decay across its surface area with an invariant slope  $s_{cone} = \frac{h_{ice}}{r_{ice}}$  as shown in Fig. 5. During these time  
 150 steps, the volume is parameterised using Eqn. 5 as:

$$V = \pi/3 \cdot r_{ice}^3 \cdot s_{cone} \quad (9)$$

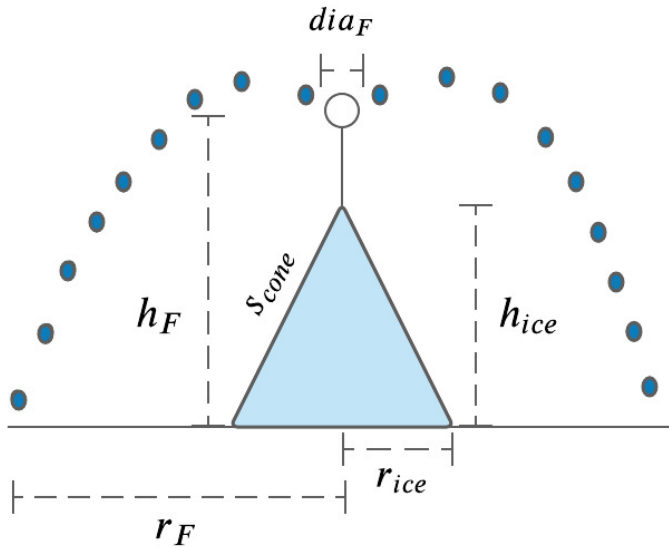


**Figure 5.** Shape and fountain parameters of the Schwarzsee Icestupa.  $r_{ice}$  is the radius,  $h_{ice}$  is the height and  $s_{cone}$  is the slope of the ice cone.  $r_F$  is the spray radius,  $h_F$  is the height and  $dia_F$  is the nozzle diameter of the fountain.

151 However, the Icestupa cannot outgrow the maximum range of the water droplets ( $(r_{ice})_{max} = r_F$ ).  
 152 Combining equations 5, 6 and 9, the geometric evolution of the Icestupa at each time step  $i$  can be  
 153 determined by considering the following rules:

$$(r_{ice}, h_{ice}) = \begin{cases} (r_F, \Delta x) & \text{if } i = 0 \\ (r_{ice}^{i-1}, \frac{3 \cdot M_{ice}}{\pi \cdot \rho_{ice} \cdot (r_{ice}^{i-1})^2}) & \text{if } r_{ice}^{i-1} \geq r_F \text{ and } \Delta M_{ice} > 0 \text{ where } \Delta M_{ice} = M_{ice}^{i-1} - M_{ice}^{i-2} \\ (\frac{3 \cdot M_{ice}}{\pi \cdot \rho_{ice} \cdot s_{cone}})^{1/3} \cdot (1, s_{cone}) & \text{otherwise} \end{cases} \quad (10)$$

### 154 3.2 Energy Balance

155 The energy balance equation for the Icestupa is formulated as follows:

$$q_{net} = q_{SW} + q_{LW} + q_L + q_S + q_F + q_G \quad (11)$$

156 where  $q_{net}$  is the net energy flux in  $[W m^{-2}]$ ;  $q_{SW}$  is the net shortwave radiation;  $q_{LW}$  is the net longwave  
 157 radiation;  $q_L$  and  $q_S$  are the turbulent latent and sensible heat fluxes.  $q_F$  represents the heat exchange  
 158 created due to the additional water and ice boundary present during fountain on time steps.  $q_G$  represents  
 159 ground heat flux between Icestupa surface and Icestupa interior. Energy transferred in the direction of the  
 160 ice surface is always denoted as positive and away as negative. Also, all temperature variables are assigned  
 161 in units of  $^{\circ}C$ .

162 Equation 11 is usually referred to as the energy budget for “the surface”, but practically it must apply to a  
 163 surface layer of ice with a finite thickness  $\Delta x$ . The energy flux acts upon the Icestupa surface layer which  
 164 has an upper and a lower boundary defined by the atmosphere and the ice body of the Icestupa, respectively.

165 The parameter selection for  $\Delta x$  is based on the following two arguments: (a) the ice thickness  $\Delta x$  should  
 166 be small enough to represent the daily surface temperature variations and (b)  $\Delta x$  should be large enough  
 167 for these temperature variations to not reach the bottom of the surface layer. Therefore, we introduced a 5  
 168 mm thick ice surface layer, over which the energy balance is calculated. A sensitivity analysis was later  
 169 performed to understand the influence of this factor. Here, we define the surface temperature  $T_{ice}$  to be  
 170 the modelled average temperature of the Icestupa surface layer and the energy flux  $q_{net}$  is assumed to act  
 171 uniformly across the Icestupa area  $A$ .

### 172 3.2.1 Net Shortwave Radiation $q_{SW}$

173 The net shortwave radiation  $q_{SW}$  is computed as follows:

$$q_{SW} = (1 - \alpha) \cdot (SW_{direct} \cdot f_{cone} + SW_{diffuse}) \quad (12)$$

174 where  $SW_{direct}$  and  $SW_{diffuse}$  are the ERA5 direct and diffuse short wave radiation,  $\alpha$  is the modelled  
 175 albedo and  $f_{cone}$  is the area fraction of the ice structure exposed to the direct shortwave radiation.

176 We model the albedo using a scheme described in Oerlemans and Knap (1998). The scheme records the  
 177 decay of albedo with time after fresh snow is deposited on the surface.  $\delta t$  records the number of time steps  
 178 after the last snowfall event. After snowfall, albedo changes over a time step,  $\delta t$ , as

$$\alpha = \alpha_{ice} + (\alpha_{snow} - \alpha_{ice}) \cdot e^{(-\delta t)/\tau} \quad (13)$$

179 where  $\alpha_{ice}$  is the bare ice albedo value and  $\tau$  is a decay rate, which determines how fast the albedo of the  
 180 ageing snow reaches this value. The decay rate  $\tau$  is assumed to have a base value of 10 days similar to  
 181 values obtained by Schmidt et al. (2017) for wet surfaces and its maximal value is set based on observations  
 182 by Oerlemans and Knap (1998) as shown in Table 1. Furthermore, the albedo  $\alpha$  varies depending on the  
 183 water source that formed the current Icestupa surface. Correspondingly, the albedo is reset to the value  
 184 of bare ice albedo if the fountain is spraying water onto the current ice surface and to the value of fresh  
 185 snow albedo if a snowfall event occurred. Snowfall events are assumed if the air temperature is below  
 186  $T_{train} = 1^{\circ}C$ .

187 The area fraction  $f_{cone}$  of the ice structure exposed to the direct shortwave radiation depends on the  
 188 shape considered. This factor is derived by calculating the area influenced by the vertical and horizontal  
 189 components of the direct solar radiation. For a conical shape, half of the total curved surface is exposed to  
 190 the vertical component of the direct shortwave radiation and the projected triangle of the curved surface  
 191 is exposed to the horizontal component of the direct shortwave radiation. The solar elevation angle  $\theta_{sun}$   
 192 used is modelled using the parametrisation proposed by Woolf (1968). Accordingly,  $f_{cone}$  is determined as  
 193 follows:

$$f_{cone} = \frac{(0.5 \cdot r_{ice} \cdot h_{ice}) \cdot \cos\theta_{sun} + (\pi \cdot r_{ice}^2 / 2) \cdot \sin\theta_{sun}}{\pi \cdot r_{ice} \cdot (r_{ice}^2 + h_{ice}^2)^{1/2}} \quad (14)$$

194 The measured diffuse shortwave radiation is assumed to impact the conical Icestupa surface uniformly.

### 195 3.2.2 Net Longwave Radiation $q_{LW}$

196 The net longwave radiation  $q_{LW}$ , for which there were no direct measurements available at Schwarzsee,  
 197 is determined as follows:

$$q_{LW} = \sigma \cdot (\epsilon_a \cdot (T_a + 273.15)^4 - \epsilon_{ice} \cdot (T_{ice} + 273.15)^4) \quad (15)$$

198 where  $T_a$  represents the measured air temperature,  $T_{ice}$  is the modelled surface temperature, both  
 199 temperatures are given in  $^{\circ}\text{C}$ ,  $\sigma = 5.67 \cdot 10^8$  is the Stefan-Boltzmann constant,  $\epsilon_a$  denotes the atmospheric  
 200 emissivity and  $\epsilon_{ice}$  is the corresponding emissivity value for the Icestupa surface (see Table 1).

201 For the calculation of the incoming longwave radiation, we approximate atmospheric emissivity  $\epsilon_a$  using  
 202 the equation suggested by Brutsaert (1982), considering air temperature and vapor pressure (Eqn. 17). The  
 203 vapor pressures over air and ice was obtained using the following formulation given in WMO (2018):

$$\begin{aligned} p_{v,a} &= 6.107 \cdot 10^{(7.5 \cdot T_a / (T_a + 237.3))} \\ p_{v,ice} &= (1.0016 + 3.15 \cdot 10^{-6} \cdot p_a - 0.074 \cdot p_a^{-1}) \cdot (6.112 \cdot e^{(22.46 \cdot T_{ice} / (T_{ice} + 272.62))}) \end{aligned} \quad (16)$$

204 where  $p_{v,a}$  denotes the saturation vapor pressure of air,  $p_{v,ice}$  denotes the saturation vapor pressure of ice  
 205 and  $p_a$  is the measured air pressure in  $[h\text{Pa}]$ . The expression defined in Brutsaert (1975) for clear skies  
 206 (first term in equation 17) is extended with the correction for cloudy skies after Brutsaert (1982) as follows:

$$\epsilon_a = 1.24 \cdot \left( \frac{p_{v,a}}{(T_a + 273.15)} \right)^{1/7} \cdot (1 + 0.22 \cdot c^2) \quad (17)$$

207 with a cloudiness index  $c$ , ranging from 0 for clear skies to 1 for complete overcast skies, obtained from  
 208 the ERA5 reanalysis data as shown in Fig. 3.

### 209 3.2.3 Turbulent sensible $q_S$ and latent $q_L$ heat fluxes

210 The turbulent sensible  $q_S$  and latent heat  $q_L$  fluxes are computed with the following expressions proposed  
 211 by Garratt (1992):

$$q_S = c_a \cdot \rho_a \cdot p_a / p_{0,a} \cdot \frac{\kappa^2 \cdot v_a \cdot (T_a - T_{ice})}{(\ln \frac{h_{AWS}}{z_{ice}})^2} \quad (18)$$

$$q_L = \begin{cases} 0.623 \cdot L_s \cdot \rho_a / p_{0,a} \cdot \frac{\kappa^2 \cdot v_a (p_{v,a} - p_{v,ice})}{(\ln \frac{h_{AWS}}{z_{ice}})^2} & \text{if } \Delta M_F = 0 \\ 0 & \text{if } \Delta M_F > 0 \text{ where } \Delta M_F = M_F^i - M_F^{i-1} \end{cases} \quad (19)$$

212 where  $h_{AWS}$  is the measurement height above the ground surface of the AWS (in  $m$ ),  $v_a$  is the wind  
 213 speed in  $[m\ s^{-1}]$  and  $M_F$  denotes fountain water spray mass in  $[kg]$ .  $c_a$  is the specific heat of air at constant  
 214 pressure ( $1010\ J\ kg^{-1}\ K^{-1}$ ),  $\rho_a$  is the air density at standard sea level ( $1.29\ kg\ m^{-3}$ ),  $p_{0,a}$  is the air pressure  
 215 at standard sea level ( $1013\ h\text{Pa}$ ),  $\kappa$  is the von Karman constant (0.4),  $L_s$  is the heat of sublimation (2848  
 216  $kJ\ kg^{-1}$ ) and  $z_{ice}$  (1.7 mm) denotes the roughness length of ice (momentum and scalar).

### 217 3.2.4 Fountain water heat flux $q_F$

218 The total energy flux is further influenced through the heat flux caused by the water that was additionally  
 219 added to the surface of the Icestupa during the time the fountain was running. We take this interaction  
 220 between the fountain water and the ice surface into account by assuming that the ice surface temperature

221 stays constantly at 0 °C during time steps when the fountain is active. This process can be divided into two  
 222 simultaneous steps: (a) the water temperature  $T_{water}$  is cooled to 0 °C and (b) the ice surface temperature is  
 223 warmed to 0 °C. Process (a) transfers hereby the necessary energy for process (b) throughout the fountain  
 224 runtime. We further assume that this process is instantaneous, i.e. the ice temperature is immediately set  
 225 to 0 °C within just one time step  $\Delta t$  when the fountain is switched on. Thus, the heat flux caused by the  
 226 fountain water is calculated as follows:

$$q_F = \begin{cases} 0 & \text{if } \Delta M_F = 0 \\ \frac{\Delta M_F \cdot c_{water} \cdot T_{water}}{\Delta t \cdot A} + \frac{\rho_{ice} \cdot \Delta x \cdot c_{ice} \cdot T_{ice}}{\Delta t} & \text{if } \Delta M_F > 0 \end{cases} \quad (20)$$

227 with  $c_{ice}$  as the specific heat of ice.

### 228 3.2.5 Bulk Icestupa heat flux $q_G$

229 The bulk Icestupa heat flux  $q_G$  corresponds to the ground heat flux in normal soils and is caused by  
 230 the temperature gradient between the surface layer and the ice body. It is expressed by using the heat  
 231 conduction equation as follows:

$$q_G = k_{ice} \cdot (T_{bulk} - T_{ice}) / l_{ice} \quad (21)$$

232 where  $k_{ice}$  is the thermal conductivity of ice in [ $W m^{-1} K^{-1}$ ],  $T_{bulk}$  is the mean temperature of the ice  
 233 body within the Icestupa and  $l_{ice}$  is the average distance of any point in the surface to any other point in the  
 234 ice body.  $T_{bulk}$  is initialised as 0 °C and later determined from Eqn. 21 as follows:

$$T_{bulk} = T_{bulk}^{i-1} - (q_G \cdot A \cdot \Delta t) / (M_{ice} \cdot c_{ice}) \quad (22)$$

235 Since we assume a conical shape with  $r_{ice} > h_{ice}$ ,  $l_{ice}$  cannot be greater than  $2r_{ice}$  and also cannot  
 236 be less than  $\Delta x$ . Therefore, the average distance from any point on the surface to any point inside is  
 237  $\Delta x \leq l_{ice} \leq r_{ice}$ . We calculate  $q_G$  here assuming  $l_{ice} = r_{ice}/2$ .

### 238 3.2.6 Surface temperature changes and melt energy $q_{melt}$

239 The available net energy  $q_{net}$  partly increases surface temperature, but also contributes to ice melt at the  
 240 surface of the Icestupa.  $q_T$  denotes the energy used on changing the surface temperature  $T_{ice}$  and  $q_{melt}$   
 241 denotes the energy used to produce meltwater. So Eqn. 11 can be rewritten as:

$$q_{net} = q_{melt} + q_T \quad (23)$$

242 The temperature fluctuates based on 3 scenarios namely, (1) the energy flux is negative but cannot freeze  
 243 all the fountain water output; (2) the energy flux is negative and can freeze all the fountain water output and  
 244 (3) the fountain is inactive ( $\Delta M_F = 0$ ). Also, the latent heat always contributes to temperature fluctuations.  
 245 Therefore, we express the rate of change of temperature as follows:

$$\frac{\Delta T}{\Delta t} = \begin{cases} -T_{ice}^{i-1} / \Delta t & \text{if } (q_{net} - q_L) < 0 \text{ and } \Delta M_F \geq -(q_{net} - q_L) \cdot A \cdot \Delta t / L_f \\ (\Delta M_F \cdot L_f) / (\rho_{ice} \cdot c_{ice} \cdot \Delta x \cdot A \cdot \Delta t) & \text{if } (q_{net} - q_L) < 0 \text{ and } \Delta M_F < -(q_{net} - q_L) \cdot A \cdot \Delta t / L_f \\ q_{net} / (\rho_{ice} \cdot c_{ice} \cdot \Delta x) & \text{if } \Delta M_F = 0 \end{cases} \quad (24)$$

246 Whenever the model predicts  $T_{ice}^{i+1} > 0^\circ C$ , then the surface temperature is set to  $0^\circ C$  in the corresponding  
 247 time step and additional energy contributes to  $q_{melt}$ . Combining these requirements, we get:

$$(q_T, q_{melt}) = \begin{cases} (\rho_{ice} \cdot c_{ice} \cdot \Delta x \cdot \frac{\Delta T}{\Delta t}, q_{net} - q_L - \rho_{ice} \cdot c_{ice} \cdot \Delta x \cdot \frac{\Delta T}{\Delta t}) & \text{if } T_{ice}^{i+1} \leq 0^\circ C \text{ and } \Delta M_F > 0 \\ (\rho_{ice} \cdot c_{ice} \cdot \Delta x \cdot \frac{\Delta T}{\Delta t}, q_{net} - \rho_{ice} \cdot c_{ice} \cdot \Delta x \cdot \frac{\Delta T}{\Delta t}) & \text{if } T_{ice}^{i+1} \leq 0^\circ C \text{ and } \Delta M_F = 0 \\ (-\rho_{ice} \cdot c_{ice} \cdot \Delta x \cdot \frac{T_{ice}^i}{\Delta t}, q_{net} - q_L + \rho_{ice} \cdot c_{ice} \cdot \Delta x \cdot \frac{T_{ice}^i}{\Delta t}) & \text{if } T_{ice}^{i+1} > 0^\circ C \text{ and } \Delta M_F > 0 \\ (-\rho_{ice} \cdot c_{ice} \cdot \Delta x \cdot \frac{T_{ice}^i}{\Delta t}, q_{net} + \rho_{ice} \cdot c_{ice} \cdot \Delta x \cdot \frac{T_{ice}^i}{\Delta t}) & \text{if } T_{ice}^{i+1} > 0^\circ C \text{ and } \Delta M_F = 0 \end{cases} \quad (25)$$

**Table 1.** Free parameters in the model categorised as constant, uncertain and site parameters. Base value (B) and uncertainty (U) were taken from the literature. For assumptions (assum.), the uncertainty was chosen to be relatively large (5 %). For measurements (meas.), the uncertainty due to parallax errors is chosen to be (1 %).

Constant Parameters	Symbol	Value	Range	References
Van Karman constant	$\kappa$	0.4	n.a.	B: Cuffey and Paterson
Stefan Boltzmann constant	$\sigma$	$5.67 \cdot 10^{-8} W m^{-2} K^{-4}$	n.a.	B: Cuffey and Paterson
Air pressure at sea level	$p_{0,a}$	1013 hPa	n.a.	B: Mölg and Hardy
Density of water	$\rho_w$	$1000 kg m^{-3}$	n.a.	B: Cuffey and Paterson
Density of ice	$\rho_{ice}$	$917 kg m^{-3}$	n.a.	B: Cuffey and Paterson
Density of air	$\rho_a$	$1.29 kg m^{-3}$	n.a.	B: Mölg and Hardy
Specific heat of water	$c_w$	$4186 J kg^{-1} ^\circ C^{-1}$	n.a.	B: Cuffey and Paterson
Specific heat of ice	$c_{ice}$	$2097 J kg^{-1} ^\circ C^{-1}$	n.a.	B: Cuffey and Paterson
Specific heat of air	$c_a$	$1010 J kg^{-1} ^\circ C^{-1}$	n.a.	B: Mölg and Hardy
Thermal conductivity of ice	$k_{ice}$	$2.123 W m^{-1} K^{-1}$	n.a.	B: Bonales et al.
Latent Heat of Sublimation	$L_s$	$2848 kJ kg^{-1}$	n.a.	B: Cuffey and Paterson
Latent Heat of Evaporation	$L_e$	$2514 kJ kg^{-1}$	n.a.	B: Cuffey and Paterson
Latent Heat of Fusion	$L_f$	$334 kJ kg^{-1}$	n.a.	B: Cuffey and Paterson
Gravitational acceleration	$g$	$9.81 m s^{-2}$	n.a.	B: Cuffey and Paterson
Uncertain Parameters				
Precipitation	$T_{rain}$	$1 ^\circ C$	$\pm 1 ^\circ C$	B + U: Fujita and Ageta, Zhou et al.
Temperature threshold				
Ice Emissivity	$\epsilon_{ice}$	0.95	$\pm 5 \%$	B: Cuffey and Paterson; U: assum.
Ice Albedo	$\alpha_{ice}$	0.35	$\pm 5 \%$	B: Cuffey and Paterson; U: assum.
Snow Albedo	$\alpha_{snow}$	0.85	$\pm 5 \%$	B: Cuffey and Paterson; U: assum.
Albedo Decay Rate	$\tau$	10 days	$[1, 22] days$	B: Schmidt et al.; U: Oerlemans and Knap assum.
Ice layer thickness	$\Delta x$	5 mm	$[1, 10] mm$	
Site Parameters				
Fountain diameter	nozzle	$dia_F$	5 mm	$\pm 1 \%$ B: meas. ; U: assum.
Fountain Height		$h_F$	1.35 m	$\pm 1 \%$ B: meas. ; U: assum.
Fountain temperature	water	$T_{water}$	$5 ^\circ C$	$[0, 9] ^\circ C$ B: meas. ; U: meas.
AWS Height		$h_{AWS}$	3 m	$\pm 1 \%$ B: meas. ; U: assum.

$$M_F + M_{ppt} + M_{dpt} = M_{ice} + M_{melt} + M_{vapour} + M_{drained} \quad (26)$$

where  $M_F$  denotes the cumulative water input;  $M_{ppt}$  is the cumulative precipitation and  $M_{dpt}$  is the cumulative accumulation through water vapour condensation or deposition;  $M_{ice}$  is the cumulative mass of ice;  $M_{melt}$  is the cumulative mass of melt water;  $M_{vapour}$  represents the cumulative water vapor loss by evaporation or sublimation and  $M_{drained}$  is the cumulative water that drains away.

Equation 26 can be rewritten using the mass balance change as:

$$\frac{\Delta M_F}{\Delta t} + \frac{\Delta M_{ppt}}{\Delta t} + \frac{\Delta M_{dpt}}{\Delta t} = \frac{\Delta M_{ice}}{\Delta t} + \frac{\Delta M_{melt}}{\Delta t} + \frac{\Delta M_{vapour}}{\Delta t} + \frac{\Delta M_{drained}}{\Delta t} \quad (27)$$

where  $\Delta M = M^i - M^{i-1}$ . Here  $\frac{\Delta M_F}{\Delta t} = d_F$  where  $d_F$  is the spray of the fountain measured in  $[kg\ s^{-1}]$ . Precipitation input is calculated as:

$$\frac{\Delta M_{ppt}}{\Delta t} = \begin{cases} \pi \cdot r_{ice}^2 \cdot \rho_w \cdot ppt & \text{if } T_a < T_{rain} \\ 0 & \text{if } T_a \geq T_{rain} \end{cases} \quad (28)$$

where  $\rho_w$  is the density of water ( $1000\ kg\ m^{-3}$ ),  $ppt$  is the measured precipitation rate in  $[m\ s^{-1}]$  and  $T_{rain}$  is the temperature threshold below which precipitation falls as snow. Here, snowfall events were identified using  $T_{rain}$  as  $1^{\circ}C$ . Snow mass input is calculated by assuming a uniform deposition over the entire circular footprint of the Icestupa.

The latent heat flux is used to estimate either the evaporation and condensation processes or sublimation and deposition processes. Deposition and sublimation involve phase change between vapour and ice whereas evaporation and condensation involve phase change between meltwater and ice. To differentiate between these two possibilities, we classify the time steps into humid or non-humid if the corresponding relative humidity value is above or below 60 % (Stigter et al., 2018). On humid time steps we assume condensation or evaporation to occur whereas on non-humid time steps deposition or sublimation can occur. Correspondingly, latent heat of evaporation ( $L_e$ ) is used for humid time steps and latent heat of sublimation ( $L_s$ ) is used for non-humid time steps. Water accumulation and vapour loss from the Icestupa surface is calculated as follows:

$$\left( \frac{\Delta M_{vapour}}{\Delta t}, \frac{\Delta M_{dpt}}{\Delta t} \right) = \begin{cases} (-q_L \cdot A/L, 0) & \text{if } q_L < 0 \\ (0, q_L \cdot A/L) & \text{if } q_L \geq 0 \end{cases} \quad (29)$$

where  $L = \begin{cases} L_e & \text{if } RH \geq 60 \\ L_s & \text{if } RH < 60 \end{cases}$

Using the melt energy  $q_{melt}$ , we estimate the frozen and melted ice mass ( $\Delta M_{ice}$ ,  $\Delta M_{melt}$ ). Removing the contribution of precipitation and combining Eqn. 29 we are left with the contribution from the melt energy as follows:

**Table 2.** Summary of calculated mass balance components for the Schwarzsee experiment after the fountain spray was stopped on 15<sup>th</sup> February 2019 and at the end of the model run on 1<sup>st</sup> April.

	Mass Component	Fountain spray ends	Model ends
Input	$M_F$	18060 kg	18060 kg
	$M_{ppt}$	439 kg	463 kg
	$M_{dpt}$	14 kg	62 kg
Output	$M_{melt}$	166 kg	1392 kg
	$M_{ice}$	1158 kg	0 kg
	$M_{vapour}$ $M_{drained}$	4 kg 17184 kg	8 kg 17184 kg

$$\left( \frac{\Delta M_{ice} - \Delta M_{ppt} - \Delta M_{dpt} + \Delta M_{vapour}}{\Delta t}, \frac{\Delta M_{melt}}{\Delta t} \right) \begin{cases} \text{if } RH < 60 \\ \left( \frac{\Delta M_{ice} - \Delta M_{ppt} - \Delta M_{dpt}}{\Delta t}, \frac{\Delta M_{melt} + \Delta M_{vapour}}{\Delta t} \right) \begin{cases} \frac{q_{melt} \cdot A}{L_f} \cdot (-1, 1) & \text{if } q_{melt} \geq 0 \\ \frac{q_{melt} \cdot A}{L_f} \cdot (-1, 0) & \text{if } q_{melt} < 0 \text{ and } \frac{\Delta M_F}{\Delta t} \geq -q_{melt} \\ \left( \frac{\Delta M_F}{\Delta t}, 0 \right) & \text{if } q_{melt} < 0 \text{ and } 0 \leq \frac{\Delta M_F}{\Delta t} < -q_{melt} \end{cases} \end{cases} \quad (30)$$

272 Now, with all the other terms known in Eqn. 27, the water drained from the Icestupa can be expressed as:

$$\frac{\Delta M_{drained}}{\Delta t} = \frac{\Delta M_F + \Delta M_{ppt} + \Delta M_{dpt} - \Delta M_{ice} - \Delta M_{melt} - \Delta M_{vapour}}{\Delta t} \quad (31)$$

273 Considering AIR as water reservoirs, we can quantify their potential through the amount of water they  
274 store (storage quantity) and the length of time they store it (storage duration). Another means of comparing  
275 different Icestupas is through their water storage efficiency defined accordingly as:

$$\text{Storage Efficiency} = \frac{M_{melt}}{(M_F + M_{ppt} + M_{dpt})} \cdot 100 \quad (32)$$

## 4 MODEL RESULTS

276 The model was forced with meteorological data from 30<sup>th</sup> January to 1<sup>st</sup> April 2019 (Fig. 3) and various  
277 parameters (see Table 1) to calculate the mass and energy balance of the Icestupa.

### 278 4.1 Energy and mass balance calculation

279 Daily averages of some components of the energy balance are shown in Fig. 6 (a). On average during the  
280 experiment duration, the total energy flux between the atmosphere and the Icestupa are almost balanced.  
281 Net shortwave radiation ( $28 \text{ W m}^{-2}$ ), sensible ( $17 \text{ W m}^{-2}$ ) and latent heat flux ( $9 \text{ W m}^{-2}$ ) with a mostly  
282 positive flux towards the surface of the icerstupa are compensated by the net longwave radiation (- 36  
283  $\text{W m}^{-2}$ ) and the melt energy (-19  $\text{W m}^{-2}$ ). The contribution of other fluxes are negligible in comparison.

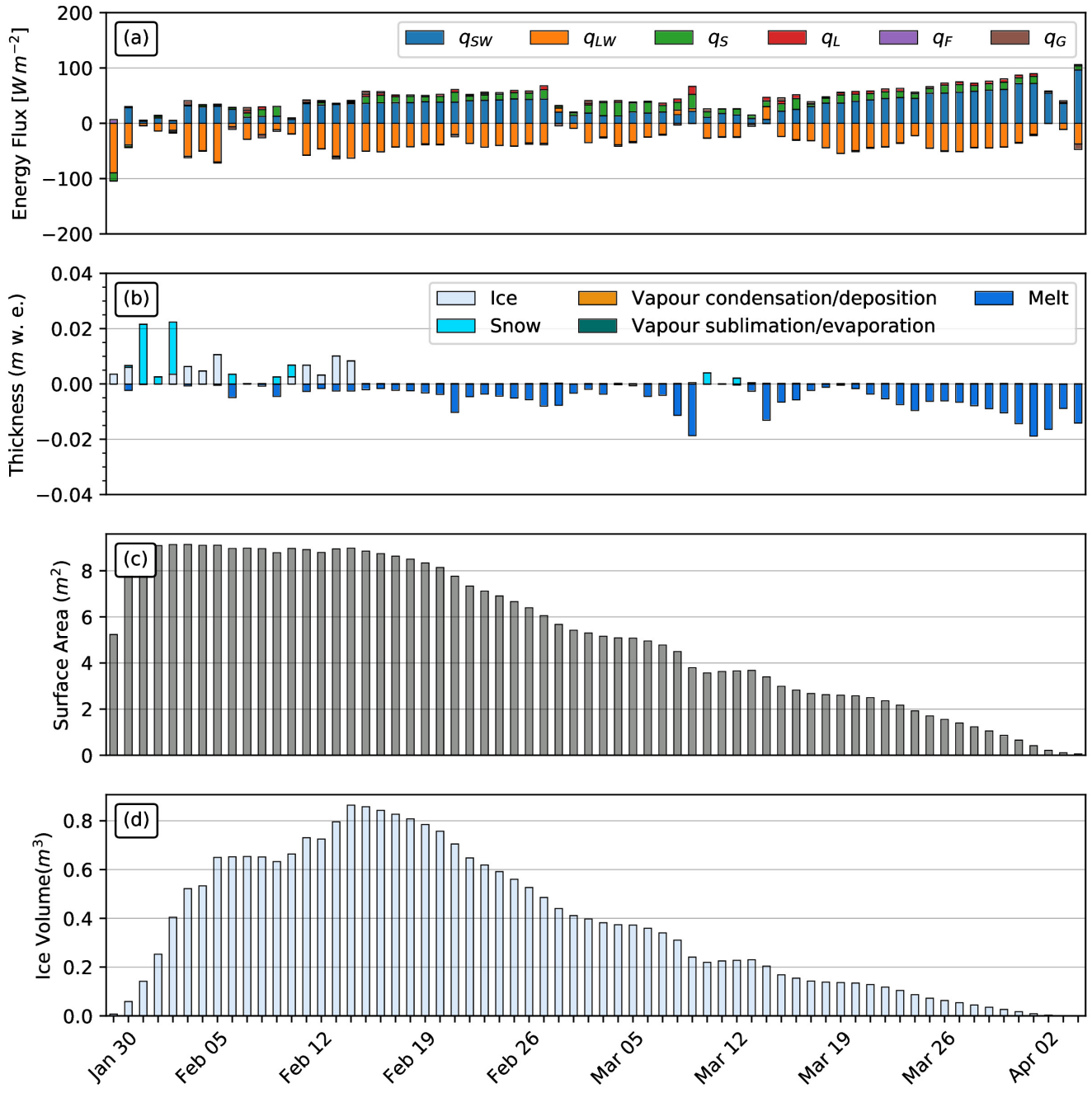


**Figure 6.** (a) Energy flux components, (b) mass flux components and (c) surface area of the Icestupa in daily time steps.  $q_{SW}$  is the net shortwave radiation;  $q_{LW}$  is the net longwave radiation;  $q_L$  and  $q_S$  are the turbulent latent and sensible heat fluxes.  $q_F$  represents the interactions of the ice-water boundary during fountain on time steps.  $q_G$  quantifies the heat conduction process between the Icestupa surface layer and the ice body.

284 Net shortwave radiation is the main input to, and the most varying energy flux on the ice surface. Its  
 285 variability is controlled by the surface albedo  $\alpha$  and the area fraction  $f_{cone}$  which therefore represent key  
 286 variables in the energy balance (Fig. 7 (a)). Although global radiation flux reached a daily maximum value  
 287 of  $304 \text{ W m}^{-2}$ ,  $q_{SW}$  only went up to  $68 \text{ W m}^{-2}$ . This is caused by the fact that only about 30 percent of  
 288 the direct solar radiation influenced the Icestupa surface as shown by the area fraction  $f_{cone}$  in Fig. 7 (a).

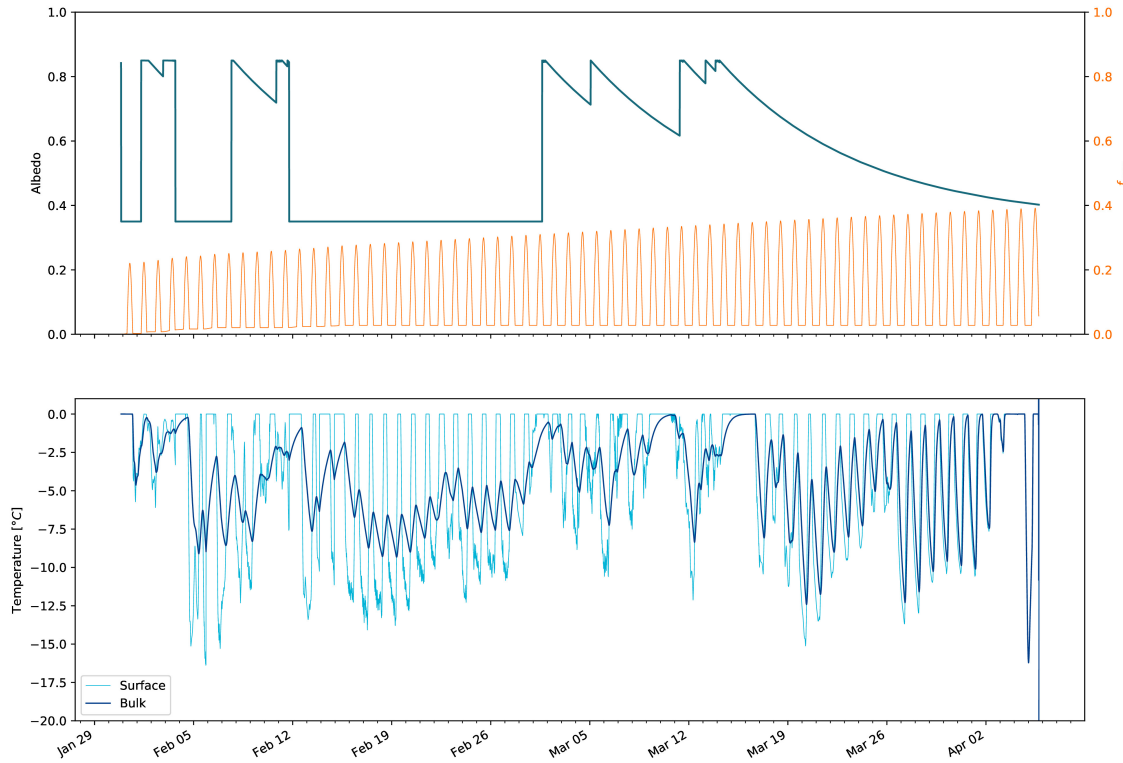


**Figure 7.** Some derived parameters of the model, namely, albedo and  $f_{cone}$  (a), Surface and bulk temperature (b). In (a), the black curve shows how snow and fountain-on events reset albedo between ice albedo and snow albedo. The decay of the snow albedo to ice albedo can also be observed. The blue curve shows how the solar radiation area fraction varied diurnally with variations in the solar elevation angle. In (b), the surface temperature (black curve) was forced to be 0 °C during fountain activity. The corresponding bulk temperature is shown with the blue curve.

289 Snowfall is the atmospheric variable connected most closely and proportionally to albedo. Higher and/or  
290 more frequent snowfall thus decreases the energy available for melt due to the corresponding increase in  $\alpha$ .

291  $q_{LW}$  was predominantly negative indicating that this energy balance component drove the freezing of the  
292 ice structure. The incoming longwave radiation was strongly dependent on atmospheric emissivity which  
293 had a mean value of 0.77. Atmospheric emissivity in turn depended on the cloudiness factor. Daily values  
294 of  $q_{LW}$  ranged from -95 to 7  $W m^{-2}$ .  $q_{LW}$  and  $q_S$  were both proportional to the temperature gradient  
295 between the air and the Icestupa surface. Turbulent sensible heat flux  $q_S$  contributed mostly to the melt  
296 of the ice structure. Daily values of  $q_S$  ranged from -16 to 59  $W m^{-2}$ . Turbulent latent heat flux  $q_L$  was  
297 predominantly positive suggesting that it favoured deposition/condensation over evaporation/sublimation.  
298 Daily values of  $q_L$  ranged from -4 to 47  $W m^{-2}$ . Therefore, the Icestupa gained mass cumulatively from  
299 the atmosphere due to the deposition/condensation process. Fountain water heat flux  $q_F$  had a mean of  
300 zero as it was only nonzero during 1002 time steps or around 100 hours. Daily values of  $q_F$  ranged from  
301 0 to 7  $W m^{-2}$ . The contribution of heat flux by conduction  $q_G$  was minimal as it only varied between  
302 -7 to 7  $W m^{-2}$  with a mean of 0  $W m^{-2}$ . The energy contributing to surface temperature changes ( $q_T$ )  
303 was insignificant in comparison to the energy spent on freezing and melting ( $q_{melt}$ ). The resulting bulk  
304 temperature and the surface temperature are shown in Fig. 7 (b). For the total considered period,  $q_{LW}$   
305 accounted for 28.3% of overall energy turnover. The energy turnover is calculated as the sum of energy

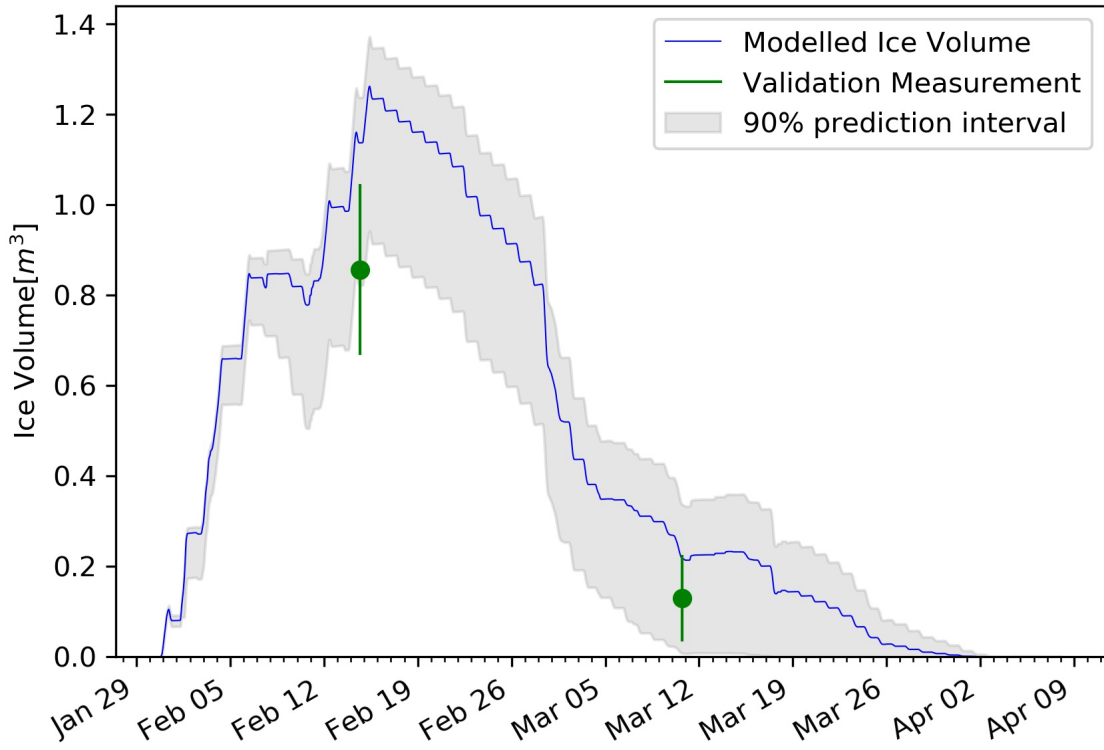


**Figure 8.** Modelled ice volume during the lifetime of the Schwarzsee Icestupa (blue curve). Green line segments indicate the first and second validation measurements. The prediction interval is based on the ice volume uncertainty caused by the most sensitive parameters, namely, temperature threshold below which precipitation falls as snow and the ice emissivity.

306 fluxes in absolute values.  $q_{SW}$  accounted for 21.7%, followed by  $q_{melt}$  (25.4%),  $q_S$  (14.6%),  $q_L$  (7.5%),  $q_G$   
307 (1.8%),  $q_F$  (0.3%) and  $q_T$  (0.3%).

308 Fig. 6 (b) represents the mass fluxes associated with these energy exchanges expressed in  $m$  w.e. It  
309 shows the ice and meltwater formed due to  $q_{melt}$ , snow accumulated due to precipitation, water vapour  
310 deposition/condensation and sublimation/evaporation due to  $q_L$ . Growth rate ( $\frac{\Delta M_{ice}}{\Delta t}$ ) shows a strong  
311 correlation with net energy flux ( $r^2 = 0.44$ ) but poor correlation with Icestupa surface area ( $r^2 = 0.04$ ).  
312 This is because the variance in growth rate is mostly due to the variance in  $q_{net}$  as illustrated in Fig. 6.  
313 Since  $r_{ice}$  was initialised with the spray radius  $r_F$ , the surface area maintains a maximum initially until the  
314 energy flux becomes positive. This trend favours the positive over the negative thickness changes resulting  
315 in a steep increase and gradual melting of ice volume as can be seen in Fig. 8.

316 The total water used for the Icestupa development includes contributions from the fountain (97.2%),  
317 snowfall (2.5 %) and deposition/condensation (0.3 %) as shown in Table 2. The maximum ice mass during  
318 the whole measurement period was 1158 kg, which occurred after the last fountain run on Feb 16<sup>th</sup> in the  
319 morning. Therefore, in the case of Schwarzsee we used a water input of 18,584 kg, with a resultant storage  
320 efficiency of only 7.5 %.

## 5 MODEL SENSITIVITY AND UNCERTAINTY ANALYSIS

321 The icestupa model can be regarded as a function  $f(x_1, x_2 \dots, x_n) = (y_1, y_2 \dots, y_m)$ , where  
322  $(x_1, x_2 \dots, x_n)$  are the model parameters and  $(y_1, y_2 \dots, y_m)$  are the model outputs. The influence of each

parameter on the output variables of interest were quantified and the most important physical parameters for the subsequent uncertainty analysis were determined. The sensitivity of a parameter  $x_j$  is determined by keeping all other parameters  $x_i, i \neq j$  fixed at their baseline value and varying  $x_j$  within values that are physically plausible.

A sensitivity study on the parameters (listed in Table 1) was performed with the maximum ice volume as the target variable. All the parameters were assumed to be independent of each other with a uniform distribution. This assumption ignores the auto-correlation present among the parameters associated with the albedo parameterisation. The range of uncertain parameters were set based on available literature values or varied  $\pm 5\%$  from the base value if no such reference was available. The uncertainty of all the site parameters were caused due to parallax errors during manual measurement. This was quantified with a range of  $\pm 1\%$  from the base value. However, it must be kept in mind that, even though intended to be as objective as possible, the selection of a parameter range has a subjective part that influences the results and conclusions obtained in this analysis. The variation of the model outputs  $y_k$  is evaluated to quantify the local sensitivities  $s_{j,k}$  that are defined here as the 95% range of the simulated outputs.

To perform the uncertainty analysis, we included only parameters that influence the maximum ice volume by at least  $0.1m^3$ . All other parameters were fixed at their baseline value. Fig. 9 shows all the variance produced by these uncertain parameters in maximum ice volume calculation. It shows that  $\epsilon_{ice}$  and  $T_{train}$  are the only parameters with a maximal sensitivity of more than  $0.1 m^3$  for the maximum ice volume estimate. Consequently, all other parameters were excluded from the subsequent uncertainty analysis.

The temperature threshold below which precipitation falls as snow ( $T_{train}$ ) was found to be the most sensitive parameter. It is used in the model to reset the albedo to snow albedo and determine snow precipitation events. The lower  $T_{train}$  parameter the higher the albedo (as the Icestupa surface has a lower albedo when ice-covered than when snow-covered). The variation of  $T_{train}$  by 5% caused maximum ice volume variation of  $1.2 \pm 0.2m^3$ .

Ice emissivity was also found to be a sensitive parameter. The higher the ice emissivity the larger the maximum ice volume as the emitted longwave radiation increases with ice emissivity. Variation of  $\epsilon_{ice}$  by 5% caused a maximum ice volume range from  $1.3 \pm 0.1m^3$ .

In total, the sensitivity analysis required 120 simulations, and the uncertainty analysis a total of 32 simulations.

## 6 DISCUSSION

### 352 6.1 Model validation quality

We first evaluate the model against the validation measurements at the Schwarzsee site. The uncalibrated model is able to capture both the freezing and the melting process sufficiently well as the modelled ice volume lies within the uncertainty of both validation measurements. Furthermore, the validation measurements fit well within the estimated model uncertainty. However, since this validation is based on only two points, it does limit the confidence in the model results. Moreover, the model seems to overestimate the ice volume at both validation points. This could be due to the underestimation of the surface area which underestimates the melt rates (absolute growth rate when  $\frac{\Delta M_F}{\Delta t} < 0$ ) and the freeze rates (absolute growth rate when  $\frac{\Delta M_F}{\Delta t} > 0$ ). However, as the fountain was mostly inactive during the study period, the underestimation of surface area disproportionately undervalues the melt rates over the freeze rates. One major cause of this underestimation was the conical shape assumption, as in reality, the Icestupa shape ranged between a cone and a cylinder (Fig. 2). Another cause was the surface irregularities that

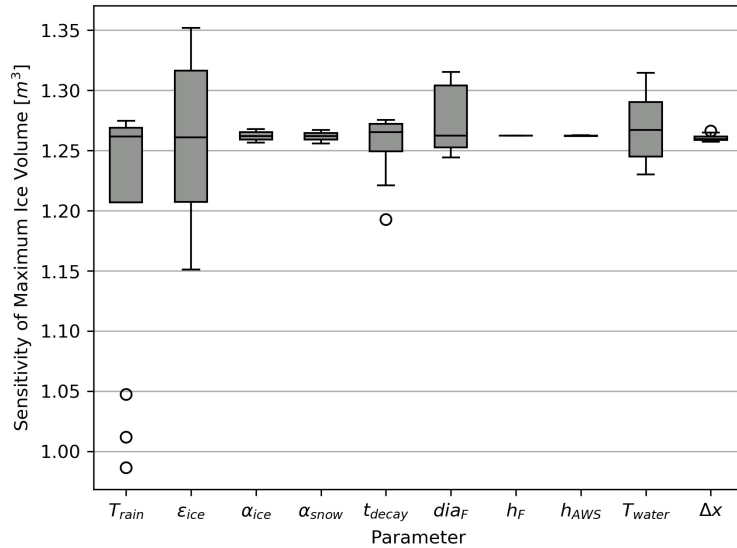


**Figure 9.** Sensitivities of maximum ice volume to all the uncertain and site parameters used in the model (Table 1). Outliers in the bar plot are shown as 'o'.

were observed due to uneven exposure to direct solar radiation and fountain droplets. The sensitivity of the model results to these errors was further amplified due to the relatively small volume of the Schwarzsee Icestupa. In summary, more validation measurements on a more voluminous Icestupa would have increased confidence on the model results.

## 6.2 Important assumptions

In the sensitivity and uncertainty analysis presented above, we did not account for several general assumptions and parametrisation choices that may cause model errors. Some assumptions and their potential to cause errors are discussed below.

- Turbulent Sensible and Latent Heat Fluxes: The method used to calculate the turbulent heat fluxes by Garratt (1992) assumes that the turbulent heat fluxes are acting over a uniform planar surface to determine the roughness length. Since our application is on a conical surface,  $z_{ice}$  has no real physical significance.
- Droplet flight time loss: Water losses during the flight time of fountain droplets were neglected making all the fountain spray available for freezing. For the Schwarzsee experiment, inclusion of this parameter does not influence results since it is already accounted for in the drained water discharge rate which was at least  $3 \text{ l min}^{-1}$ .
- Nucleation of droplets: Corresponding to droplet flight time, ice/snow formation is also possible before surface contact if nucleation occurs during flight time. For the Schwarzsee experiment, this process will further increase the freeze rate and hence the storage efficiency. This process is neglected for model simplicity.

## 6.3 Schwarzsee vs Ladakh Icestupa

It could be argued that the relatively small Schwarzsee Icestupa cannot be compared with the much larger Icestupas in Ladakh which store millions of litres of water for several months (see Appendix 8.1). However, this is the only Icestupa dataset available for such a model validation.

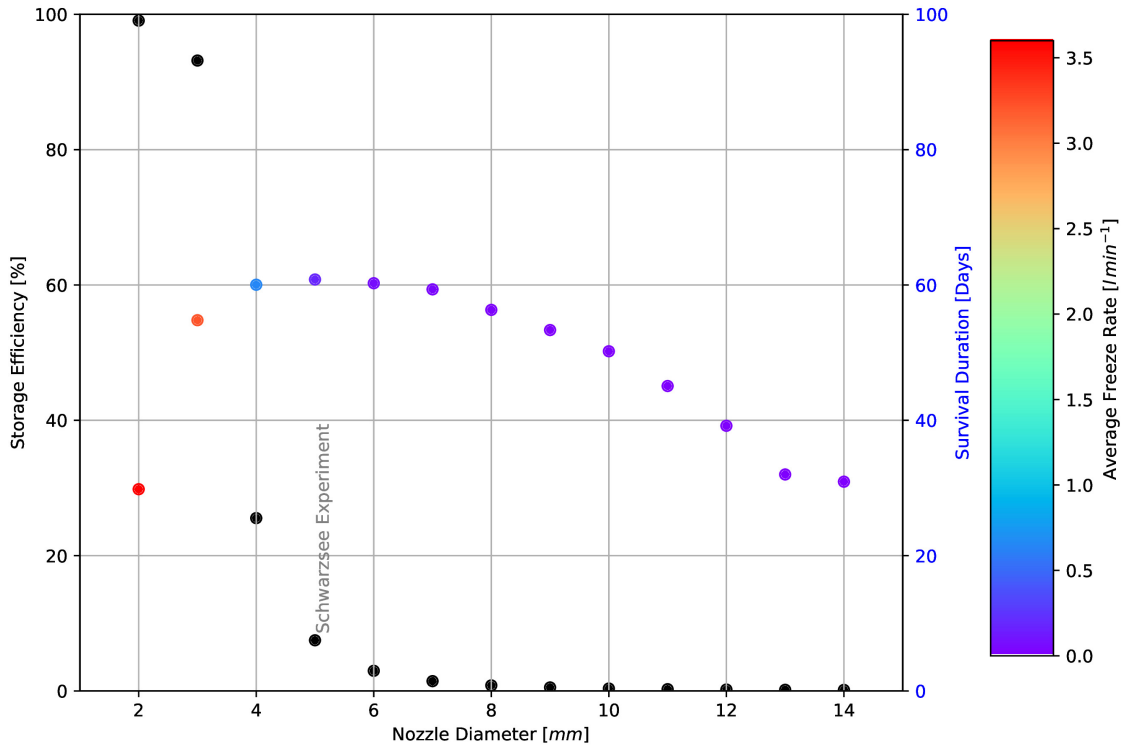


**Figure 10.** Variation in storage efficiency (black dots) and storage duration (coloured dots) with changes in fountain nozzle's nozzle diameter. The dot colours represent average freeze rate based on the color bar.

388 Table 2 clearly shows that for our Schwarzsee experiment most of the input water (92 %) simply drained  
 389 away. This high water loss through drainage is due to the fact that the average spray rate of the fountain  
 390 ( $(\frac{\Delta \dot{M}_F}{\Delta t})_{mean} = 3.6 l min^{-1}$ ) far exceeded the max Icestupa growth rate ( $(\frac{\Delta M_{ice}}{\Delta t})_{max} = 1 l min^{-1}$  (w.e.) ).

391 In the city of Leh, Ladakh at an altitude of 3500 m a.s.l. the air temperature shows values down to  
 392 27.9 °C in winter (Chevuturi et al., 2018) whereas Schwarzsee had a minimum temperature of just -11.6  
 393 °C during the study period. Moreover, subzero temperatures were only reached for 7 nights of fountain  
 394 operation at the Schwarzsee site compared to the 43 nights of fountain operation possible in Ladakh (see  
 395 Appendix 8.1). Thus, the Icestupa growth rate is expected to be much higher in Ladakh. However, water  
 396 spray rates in Ladakh are also much higher (around  $210 l min^{-1}$ ). So the water losses in Ladakh could  
 397 also be caused due to excessive fountain spray.

#### 398 6.4 Icestupa construction decisions

399 There are several decisions one has to take when constructing Icestupas. These can be broadly divided  
 400 into two types of decisions, namely fountain and location decisions. Both the meteorological conditions  
 401 of the location and the surface area produced by the fountain significantly influence the observed growth  
 402 rate. Since our validation is restricted to just one location, we restrict our discussion to the optimization  
 403 possibilities of Icestupa constructions through fountain decisions.

404 Assuming a constant spray for the fountain, we can divide the fountain decisions into fountain state  
 405 (on/off) and type (height and nozzle diameter). From an energy balance point of view, the fountain should  
 406 be switched on for all time intervals when  $q_{net} < 0$ . However, in our experiment, the fountain state decision  
 407 was set based on whether the ambient temperature was above or below a critical temperature of  $-5^{\circ}C$ .  
 408 Ambient temperature can serve as an indicator of  $q_{net}$  as it was correlated ( $r^2 = 0.53$ ). However,  $q_{net}$

409 was found to be negative already at a critical temperature of  $-1^{\circ}\text{C}$ . Therefore, using air temperature to  
410 determine when the fountain should be switched on is justified but a higher critical temperature could have  
411 been used in the case of the Schwarzsee Icestupa.

412 The fountain type used can be characterised by the physical structure of the fountain, namely its height and  
413 nozzle diameter. Maintaining the same spray rate and height, one can optimize the Icestupa development  
414 by identifying the minimum nozzle diameter that yields the maximum storage efficiency.

415 Fig. 10 shows reducing the nozzle diameter to  $3\text{ mm}$  increases storage efficiency up to 93 % without  
416 compromising much on storage duration. The corresponding storage quantity of the  $3\text{ mm}$  nozzle diameter  
417 was more than 20 times higher than the  $5\text{ mm}$  fountain used in our experiment. This is because the spray  
418 radius  $r_F$  of the  $3\text{ mm}$  fountain was much higher at  $8.5\text{ m}$  compared to the  $1.7\text{ m}$  spray radius of the  
419  $5\text{ mm}$  fountain (see Appendix Section ??). Here, we define growth rate as freeze rate when fountain is  
420 active and melt rate otherwise. So this higher spray radius both, increases the freeze rate and increases  
421 the melt rate since they are both directly proportional to the surface area. However, since the freeze rate  
422 cannot increase beyond a spray rate of  $3.6\text{ l min}^{-1}$  (except during precipitation or deposition/condensation  
423 events), an optimum spray radius or nozzle diameter exists, beyond which storage duration suffers due to a  
424 disproportionate increase in melt rate compared to the freeze rate. So even though  $3\text{ mm}$  nozzle diameter  
425 had a much higher storage quantity than the  $5\text{ mm}$  nozzle, its storage duration was around 6 days lesser  
426 than the  $5\text{ mm}$  nozzle. One physical cause of this effect is the different shapes of both the ice structures. A  
427 flat sheet of ice (effectively a cone with a high spray radius) with higher mass might have a storage duration  
428 shorter than a conical ice structure. As the spray radius decreases with increasing nozzle diameter, the ice  
429 structure's average slope increases and so the  $5\text{ mm}$  nozzle's ice structure is "more" conical than the  $3\text{ mm}$   
430 ice structure. Fig. 10 shows that a nozzle diameter of  $3\text{ mm}$  has an average freeze rate ( $3.2\text{ l min}^{-1}\text{w.e.}$ )  
431 which is large enough to increase the storage efficiency and small enough to not reduce the storage duration  
432 of the Icestupa significantly.

## 7 CONCLUSIONS

433 We outlined a methodology for estimating ice, liquid water, water vapour and drained quantities produced  
434 during the construction of an Icestupa using measurements of fountain spray rate, air temperature, radiation,  
435 humidity, pressure, wind and cloudiness at the Schwarzsee study site. The comparison with validation  
436 measurements at two different dates during the experiment led to satisfying results, although a more  
437 rigorous model validation was not possible due to few icestupa volume measurements.

438 According to the model, the Schwarzsee Icestupa achieved a storage quantity of 1392 litres of water with  
439 a storage duration of 61 days. However, the corresponding storage efficiency was very low with only 7.5 %  
440 for a water input of 18,584 litres. These estimates were most sensitive to the temperature threshold that  
441 determined precipitation phase and ice emissivity parameters which created an uncertainty of  $1.2 \pm 0.3\text{ m}^3$   
442 in the maximum ice volume calculated. This is to be expected as net longwave radiation and net shortwave  
443 radiation together accounted for around 50 % of the overall energy turnover.

444 Although the location, storage quantity and duration of our experimental Schwarzsee Icestupa are not  
445 representative of the much larger Icestupas of Ladakh, the model results do support the hypothesis that  
446 there could be considerable water loss during the formation of Icestupas particularly due to excessive  
447 fountain spray. Using model calculations, it was shown that a decreased fountain nozzle diameter of  $3\text{ mm}$   
448 can increase the storage efficiency drastically. This is because a change in the fountain nozzle diameter  
449 causes an effective change of the ice surface area over which the net energy flux can act. This result has  
450 relevance on the future design of Icestupa fountains. However, care has to be taken as our model is currently

451 only validated by one experiment at the Schwarzsee site. Further experiments at different locations with  
452 different fountains are required to better understand the influence of construction decisions on the results.

## 8 APPENDIX

### 453 8.1 Ladakh Icestupa 2014/15

454 A 20 m tall Icestupa (Wangchuk, 2015c) was built in Phyang village, Ladakh at an altitude of 3500  
455 m a.s.l. Assuming a conical shape with a diameter of 20 m, the corresponding volume of this Icestupa  
456 becomes 2093 m<sup>3</sup> or 1,919,587 litres w.e. The fountain sprayed water at a rate of 210 l min<sup>-1</sup> (Wangchuk,  
457 2015e) from 21<sup>st</sup> January (Wangchuk, 2015a) to at least until 5<sup>th</sup> March 2015 (Wangchuk, 2015b) (around  
458 43 nights). Assuming fountain spray was active for 8 hours each night, we estimate water consumption to  
459 be around 4,334,400 litres. So just during construction/freezing period of the Icestupa, roughly 56 % of the  
460 water provided was wasted. The actual water loss is bound to be much higher due to further vapour losses  
461 during the melting period. This Icestupa completely melted away on 6<sup>th</sup> July 2015 (Wangchuk, 2015d).  
462 Therefore, the storage duration was 166 days or roughly 5 months.

## CONFLICT OF INTEREST STATEMENT

463 The authors declare that the research was conducted in the absence of any commercial or financial  
464 relationships that could be construed as a potential conflict of interest.

## AUTHOR CONTRIBUTIONS

465 SB wrote the initial version of the manuscript. MH, ML, SW, JO, and FK commented on the initial  
466 manuscript and helped improve it. SB developed the methodology with inputs from MH. SB performed the  
467 analysis with support from MH and ML. SB and MH participated in the fieldwork.

## FUNDING

468 This work was supported and funded by the University of Fribourg and by the Swiss Government Excellence  
469 Scholarship (Suryanarayanan Balasubramanian).

## ACKNOWLEDGMENTS

470 We thank Mr. Adolf Kaeser and Mr. Flavio Catillaz at Eispalast Schwarzsee for their active participation  
471 in the fieldwork. We would also like to thank Digmesa AG for subsidising their flowmeter used in the  
472 experiment. We would particularly like to thank the editor Prof. Thomas Schuler who gave us important  
473 inputs to improve the paper and we thank also Prof. Christian Hauck and Prof. Nanna B. Karlsson for  
474 valuable suggestions that improved the manuscript.

## DATA AVAILABILITY STATEMENT

475 The data and code used to produce results and figures will be published at a later stage and can, until then,  
476 be obtained from the authors upon request.

## REFERENCES

- 477 Apel, H., Abdykerimova, Z., Agalhanova, M., Baimaganbetov, A., Gavrilenko, N., Gerlitz, L., et al. (2018).  
478 Statistical forecast of seasonal discharge in central asia using observational records: development of a  
479 generic linear modelling tool for operational water resource management. *Hydrology and Earth System*  
480 *Sciences* 22, 2225–2254. doi:10.5194/hess-22-2225-2018

- 481 Bonales, L. J., Rodriguez, A. C., and Sanz, P. D. (2017). Thermal conductivity of ice prepared under  
482 different conditions. *International Journal of Food Properties* 20, 610–619. doi:10.1080/10942912.  
483 2017.1306551
- 484 Brutsaert, W. (1975). On a derivable formula for long-wave radiation from clear skies. *Water Resources  
485 Research* 11, 742–744. doi:10.1029/WR011i005p00742
- 486 Brutsaert, W. (1982). *Evaporation into the Atmosphere. Theory, History and Application* (Kluwer Academic  
487 Publishers)
- 488 Buck, A. L. (1981). New equations for computing vapor pressure and enhancement factor. *Journal of  
489 Applied Meteorology and Climatology* 20, 1527 – 1532
- 490 Buytaert, W., Moulds, S., Acosta, L., Bievre, B. D., Olmos, C., Villacis, M., et al. (2017). Glacial melt  
491 content of water use in the tropical andes. *Environmental Research Letters* 12, 114014. doi:10.1088/  
492 1748-9326/aa926c
- 493 Chen, Y., Li, W., Deng, H., Fang, G., and Li, Z. (2016). Changes in central asia's water tower: Past, present  
494 and future. *Nature* doi:10.1088/1748-9326/aa926c
- 495 Chevuturi, A., Dimri, A. P., and Thayyen, R. J. (2018). Climate change over leh (ladakh), india. *Theoretical  
496 and Applied Climatology* 131, 531–545. doi:10.1007/s00704-016-1989-1
- 497 [Dataset] Copernicus Climate Change Service (C3S) (2017). Era5: Fifth generation of ecmwf atmospheric  
498 reanalyses of the global climate
- 499 Cuffey, K. M. and Paterson, W. S. B. (2010). *The Physics Of Glaciers* (Elsevier)
- 500 Fujita, K. and Ageta, Y. (2000). Effect of summer accumulation on glacier mass balance on the  
501 tibetan plateau revealed by mass-balance model. *Journal of Glaciology* 46, 244–252. doi:10.3189/  
502 172756500781832945
- 503 Garratt, J. R. (1992). *The Atmospheric Boundary Layer* (Cambridge University Press)
- 504 Grossman, D. (2015). As himalayan glaciers melt, two towns face the fallout
- 505 Hersbach, H., Bell, B., Berrisford, P., Hirahara, S., Horányi, A., Muñoz-Sabater, J., et al. (2020). The era5  
506 global reanalysis. *Quarterly Journal of the Royal Meteorological Society* 146, 1999–2049
- 507 Hock, R., Rasul, G., Adler, C., Cáceres, B., Gruber, S., Hirabayashi, Y., et al. (2019). 2019: High mountain  
508 areas. *IPCC Special Report on the Ocean and Cryosphere in a Changing Climate* [H.-O. Pörtner, D.C.  
509 Roberts, V. Masson-Delmotte, P. Zhai, M. Tignor, E. Poloczanska, K. Mintenbeck, A. Alegria, M. Nicolai,  
510 A. Okem, J. Petzold, B. Rama, N.M. Weyer (eds.)]
- 511 Hoelzle, M., Barandun, M., Bolch, T., Fiddes, J., Gafurov, A., Muccione, V., et al. (2019). *The status and  
512 role of the alpine cryosphere in Central Asia*. doi:10.4324/9780429436475-8
- 513 [Dataset] IDAWEB (2019). Meteoswiss, federal office of meteorology and climatology
- 514 Immerzeel, W. W., Lutz, A. F., Andrade, M., Bahl, A., Biemans, H., Bolch, T., et al. (2019). Importance  
515 and vulnerability of the world's water towers. *Nature* 577, 364 – 369. doi:10.1038/s41586-019-1822-y
- 516 Meteoblue (2020). Climate schwarzsee
- 517 Mölg, T. and Hardy, D. R. (2004). Ablation and associated energy balance of a horizontal glacier surface  
518 on kilimanjaro. *J. Geophys. Res.-Atmos.* 109, 1–13. doi:10.1029/2003JD004338
- 519 Nüsser, M., Dame, J., Kraus, B., Baghel, R., and Schmidt, S. (2019a). Socio-hydrology of artificial glaciers  
520 in ladakh, india: assessing adaptive strategies in a changing cryosphere. *Regional Environmental Change*  
521 doi:10.1007/s10113-018-1372-0
- 522 Nüsser, M., Dame, J., Parveen, S., Kraus, B., Baghel, R., and Schmidt, S. (2019b). Cryosphere-Fed  
523 Irrigation Networks in the Northwestern Himalaya: Precarious Livelihoods and Adaptation Strategies  
524 Under the Impact of Climate Change. *Mountain Research and Development* 39. doi:10.1659/  
525 MRD-JOURNAL-D-18-00072.1

- 526 Oerlemans, J. and Knap, W. H. (1998). A 1 year record of global radiation and albedo in the  
527 ablation zone of morteratschgletscher, switzerland. *Journal of Glaciology* 44, 231–238. doi:10.  
528 3189/S0022143000002574
- 529 Schmidt, L. S., Aðalgeirsdóttir, G., Guðmundsson, S., Langen, P. L., Pálsson, F., Mottram, R., et al. (2017).  
530 The importance of accurate glacier albedo for estimates of surface mass balance on vatnajökull: evaluating  
531 the surface energy budget in a regional climate model with automatic weather station observations. *The  
532 Cryosphere* 11, 1665–1684. doi:10.5194/tc-11-1665-2017
- 533 Stigter, E. E., Litt, M., Steiner, J. F., Bonekamp, P. N. J., Shea, J. M., Bierkens, M. F. P., et al. (2018).  
534 The importance of snow sublimation on a himalayan glacier. *Frontiers in Earth Science* 6, 108.  
535 doi:10.3389/feart.2018.00108
- 536 Tetens, O. (1930). Über einige meteorologische begriffe. z. *Geophys.* 6, 297–309
- 537 Unger-Shayesteh, K., Vorogushyn, S., Farinotti, D., Gafurov, A., Duethmann, D., Mandychev, A., et al.  
538 (2013). What do we know about past changes in the water cycle of central asian headwaters? a review.  
539 *Global and Planetary Change* 110, 4 – 25. doi:10.1016/j.gloplacha.2013.02.004. Water in Central Asia  
540 – Perspectives under global change
- 541 Wangchuk, S. (2014). Ice stupa artificial glaciers of ladakh
- 542 Wangchuk, S. (2015a). The good news at ice stupa 24th january 2015
- 543 Wangchuk, S. (2015b). Ice stupa artificial glacier inaugurated 5th of march 2015
- 544 Wangchuk, S. (2015c). Ice stupa surpasses guiness world record
- 545 Wangchuk, S. (2015d). Ice stupa way of celebrating a special day
- 546 Wangchuk, S. (2015e). World water day at ice stupa
- 547 WMO (2018). *Guide to Instruments and Methods of Observation* (World Meteorological Organization ;  
548 2018 (2018 Edition))
- 549 Woolf, H. M. (1968). *On the Computation of Solar Elevation Angles and the determination of sunrise and  
550 sunset times* (National Aeronautics and Space Administration)
- 551 Zhou, S., Kang, S., Gao, T., and Zhang, G. (2010). Response of zhadang glacier runoff in nam co basin,  
552 tibet, to changes in air temperature and precipitation form. *Chinese Science Bulletin* 55, 2103–2110.  
553 doi:10.1007/s11434-010-3290-5